Available online at www.ijournalse.org

Emerging Science Journal

(ISSN: 2610-9182)

Vol. 9, No. 2, April, 2025

High-Sensitivity Toxic Gas Sensor Utilizing Photonic Crystal Fibers in the THz Spectrum

Mir Sabbir Hossain [1], Ariyan Haque Joy [1], Diponkar Kundu [1], A. H. M. Iftekharul Ferdous [1*], Abdullah Al Mamun [2, 3], Md Jakir Hossen [4*]

[1] *Department of Electrical and Electronic Engineering, Pabna University of Science and Technology, Pabna 6600, Bangladesh.*

[2] *Department of Electrical and Electrical Engineering, Feni University, Feni-3900, Bangladesh.*

[3] *School of Information and Communication Technology, Griffith University, Queensland, 4111, Australia.*

[4] *Faculty of Engineering and Technology, Multimedia University, Melaka-75450, Malaysia.*

Abstract

SO_2, HCN, and Cl_2 gases are extremely toxic and can present significant health hazards even at minimal amounts, including respiratory and neurological systems. Timely identification aids in averting exposure and alleviating possible health risks, particularly in industrial and densely populated regions. Moreover, these gases can contribute to environmental pollution; thus, their monitoring is essential for human safety and environmental preservation. This specification recommends employing a photonic crystal fiber (PCF) to construct a terahertz octagonal core and curved air hole sensor for the detection of SO2, HCN, and Cl_2 in the THz region. We routinely evaluate the recommended framework numerically, utilizing the entire finite element method. In terms of Cl_2, the recommended sensor has a larger numerical aperture of 0.2909 and a superior sensitivity of 99.58%. Furthermore, this simulation yields a reduced effective material loss equal to 0.0020 cm^{-1} with a 3.094×10^{-12} dB/m confinement loss for this gas. This technology utilizes the distinctive interaction between THz vibrations and gas molecules, improving detection sensitivity at trace levels relative to other techniques. This type of sensor may have practical applications in chemical sensing, biosensing, and gas sensing.

Keywords:

Sulfur Dioxide;

Hydrogen Cyanide;

Chlorine;

Sensor Sensitivity;

Finite Element Method (FEM).

Article History:

Received:	14	September	2024
Revised:	25	February	2025
Accepted:	07	March	2025
Published:	01	April	2025

1- Introduction

In the atmosphere, sulphur dioxide is a highly conventional pollutant. Typically, it is ejected through the combustion of sulphur-containing coal and oil, as well as the melting of various ores. Because of its exalted ability to dissolve in water, sulphur dioxide plays a role in the production of acid aerosol (H_2SO_4), which causes acid rain or acid accumulation that can harm historic structures, trees, crops, and other bodies of water [1]. Exposure to a significant quantity of weather containing SO_2 can harm the respiratory system of our body, causing signs like sneezing, coughing, or even difficulty breathing. Prolonged exposure might exacerbate pre-existing respiratory conditions, such as severe asthma and bronchitis. Prolonged exposure to high levels of SO_2 is linked to the development of respiratory and cardiovascular conditions. Children, older individuals, and individuals with pre-existing medical conditions are the groups who are most vulnerable [2]. The cyano band (C≡N) includes hydrogen cyanide (HCN), a hazardous chemical agent that exists as an uncolored gas. Hydrogen cyanide prevents cells and tissues from carrying out their normal respiration processes. It firmly

* **CONTACT**: iferdous.eee@pust.ac.bd; jakir.hossen@mmu.edu.my

DOI: http://dx.doi.org/10.28991/ESJ-2025-09-02-01

binds the iron atoms to the haemoglobin in the bloodstream. Because of this, haemoglobin fails to carry oxygen (O_2) to the body's respiratory tissues [3]. Cl_2 (chlorine) is a very bothersome gas, as well as a reactive gas that can pose a risk to human health and the environment. Exposure to a high concentration of Cl_2 causes severe damage to the cells lining the lungs, increases the sensitivity of the airways, reduces the ability to remove fluid from the air sacs, and causes fluid accumulation in the lungs when there is a higher level of inflammation and a large amount of neutrophils accumulating in the lungs [4]. Detection of SO_2 using Polymer Vesicle Sensors [5], Cl_2 using 2D PbSe/Bi_2Se_3 Heterojunctions [6], and cyanide by colorimetric and fluorogenic sensors [7].

Although colorimetric/fluorogenic sensors, polymer vesicle sensors, and 2D PbSe/Bi_2Se_3 heterojunctions have all been used to detect SO_2, Cl_2, and cyanide, each technique has drawbacks. The accuracy and longevity of polymer vesicle sensors for SO_2 detection are commonly impacted by their instability in a variety of environmental situations and potential degradation over time. Despite their sensitivity, the 2D PbSe/Bi_2Se_3 hetero-junctions for Cl_2 detection have scalability issues and are susceptible to temperature and humidity variations, which can cause variations in detection accuracy. Similar limitations exist for cyanide detection employing colorimetric and fluorogenic sensors, which can compromise accuracy and selectivity in complex combinations due to their susceptibility to external light conditions and possible interference from other ions or compounds, despite their high specificity. Collectively, these limitations highlight the need for a more stable, sensitive, and interference-resistant detection approach. Various techniques for detecting harmful gases have been presented thus far; nevertheless, they all suffer certain drawbacks, including lengthy analysis times, complex procedures, and the requirement for a skilled operator. In order to enhance the precision of gas detections and improve their usability, researchers have put forward several novel sensing techniques [8-10].

Photonic crystal fiber is gaining popularity among photonics researchers as a technology for sensor design because of its configurable properties in the interaction between light and matter. By adjusting certain design parameters such as the shape of the air holes, the distance between them, and the diameter of the core, one can minimize confinement loss, absorption loss, and birefringence, and control dispersion. These adjustments are not possible with conventional optical fibers. By adjusting the geometrical adaptation of holes and using the right materials, we can utilize PCF for specific applications like chemical sensors and optical communications [11, 12]. PCF is a type of fiber optic that has a photonic crystal cladding encircling the cable core. Throughout the fiber, an ordinary pattern of microscopic air holes creates a periodic, low-loss dielectric medium called a photonic crystal. The cladding's and the core's differing refractive indices create a refraction feature that allows light to pass through the core. The PCF's core centers light, delivering photons to a far more powerful waveguide than they would in an ordinary fiber optic system. Polymers, not glass, form the PCF, simplifying and lowering the cost of manufacturing a more durable fiber [13]. Multiple PCF types exist depending on the core's solid, hollow, or porous nature. As it offers a core region with a larger analyte volume than other core types, we have selected HC-PCF within all these types of fibers for sensing purposes [14]. PCF-based sensors are widely used because of their dynamic qualities, which include toughness, compact shapes and sizes, excellent sensitivity, cost-effectiveness, and the capacity to respond in challenging environments like areas with excessive chemical exposure as well as elevated electromagnetic fields. These sensors have outstanding applications in chemical, vapor, and gas sensing, communication, environmental analysis, bioprocess control, and medical fields, among others [15-17]. The range of frequencies from 0.1 to 10 THz (0.003–3 mm) is referred to as terahertz, and it is considered one of the most affirmative spectral areas because of its possible utilization in various fields, including imaging [18], communications [19], security monitoring [20], and biomedical diagnosis [21]. Because it is situated within the range that lies between the infrared and microwave spectrums, the terahertz region transmits characteristics of both [22].

Over the past few years, numerous studies in the domain of chemical sensing have gained attention. Arif et al. [23] recommended chemical sensing designs that yielded a 58.5% sensitivity. Mohamed Nizar et al. [24] devised a highly sensitive PCF detector for identifying sulphur dioxide (SO_2) with a maximum RS (relative sensitivity) of 59.34%. In early 2019, Podder et al. [25] created a photonic crystal fiber framework to detect sulfuric acid that achieved a maximum sensitivity of 63.4%. Sultana et al. [26] proposed a PCF with an elliptical core, specifically designed for ethanol identification, in 2018. Operating at a frequency of 1 THz, the recommended design provides the highest sensitivity, equal to 68.87%, while having a CL equal to 7.79×10^{-12} cm^{-1}. Abbaszadeh et al. [27] introduced a photonic crystal fiber gas sensor that detects ammonia in 2022. The sensor utilized a circular ring-based microstructure core and achieved a remarkable relative sensitivity of 70.25%. In 2022, Nizar et al. [28] developed a sensor using photonic crystal fiber to detect dangerous chemicals. The sensor demonstrated a peak sensitivity of 75.75%. Islam et al. (2018) [3] presented a PCF design featuring an elliptical form for the airhole in the core. This design achieved a RS equal to 77.5% as well as a CL equal to 5.5×10^{-7} cm^{-1}. Ahmed et al. [29] developed a terahertz detector for identifying components of blood using a PCF design in 2018. They constructed the PCF using hexagonally arranged cladding as well as a crystalline core of type B that achieved a peak sensitivity equal to 80.56%. Islam et al. [30] obtained a sensitivity equal to 85.8% by utilizing their custom-designed PCF operating in the THz frequency range. Islam et al. [31] developed a photonic sensor using Zeonex material to detect alcohol that has a remarkably excellent RL equal to 88.6%. Mahmud et al. [32] introduced a chemical sensor for detecting toxic substances utilizing PCF in 2019. The sensor features an octagonal-shaped hollow core with an exalted RS of 92.08% at a 1.4 THz frequency.

Hossain et al. [33] created a rectangular HC-PCF design for identifying harmful chemicals in 2020. This proposed design obtains a sensitivity equal to 94.4% with a CL of 1.71×10^{-14} cm^{-1} at 1.8 terahertz frequency, which is the highest sensitivity achieved. Islam et al. [14] introduced a chemical sensing device using a hollow-core photonic crystal fiber for terahertz frequencies in 2018. This sensor achieved a remarkable sensitivity of 96.8% at a frequency of 1.4 THz. In 2024, Hossain et al. [34] proposed design and performance evaluation of a photonic crystal fiber (PCF)-based octagonal chemical sensor for the detection of benzene, ethanol, and water within the terahertz band, achieving a responsivity of 93.80%. As early as 2024, Mahbub et al. [35] suggested gas detection utilizing soliton effect pulse compression with an RS of 64%. In same, Ferdous et al. [2] conducted research on the detection of SO2, achieving a sensitivity of 87.39% and a confinement loss of 6.8194×10^{-4} dB/m. In 2024, Pourfathi Fard et al. [36] proposed a concept for a Photonic Crystal Fiber intended for the detection of Hydrogen Cyanide gas, with a relative sensitivity of 65.13% and a minimal confinement loss of 1.5×10^{-3} dB/m. In 2024, Islam et al. [37] proposed a photonic crystal fiber design for cyanide gas detection. This design has an RS of 99.62% and a low confinement loss of 5.88×10^{-09} dB/m. However, it is capable of detecting NaCN and KCN, not HCN. The research gaps are the sensitivity of multiple toxic gases, innovative core structures and materials, and the enhancement of confinement loss (CL). To the best of our knowledge, research should be conducted on the detection of such gasses utilizing photonic crystal fibers in the terahertz domain. This research proposes the utilization of an HC-PCF sensing in the THz frequency region for the detection of poisonous gases, including SO_2, HCN, and Cl_2, which can be lethal.

The performance is assessed by evaluating several optical parameters. We evaluate several optical parameters to assess the performance. Upon examining the optical characteristics, specifically relative sensitivity, confinement loss (CL), effective material loss (EML), spot size (SS), and numerical aperture (NA), we confidently state that this sensing will outperform previous studies. Consequently, there is a growing requirement to create innovative methods for quickly, accurately, and sensitively identifying toxic gases. The primary goal of creating a high-sensitivity hazardous gas sensor using photonic crystal fiber's (PCF) in the terahertz (THz) band is stated in the text quite clearly. The goal of the project is to develop a novel PCF structure that is tailored for the THz spectrum in order to overcome the shortcomings of traditional toxic gas sensors and detect dangerous chemicals including SO_2 , HCN, and Cl_2 with remarkable precision and dependability. The article's goal is to get minimal confinement loss (CL) and increased sensitivity, both of which are essential for identifying traces of hazardous gases in environmental and industrial contexts. The goal is highlighted by contrasting the performance of the suggested sensor with that of current designs, demonstrating its improved sensitivity and efficiency and highlighting its potential for useful, high-precision gas detection applications.

In Section 2, we will provide a comprehensive analysis of our methodology, which will include a detailed description of the design and optimization process of our high-sensitivity photonic crystal fiber (PCF) sensor, which is specifically designed for the detection of toxic gases in the terahertz (THz) spectrum. The analytical and simulation techniques used to assess the sensor's performance parameters, including relative sensitivity (RS) and confinement loss (CL) for target gases SO_2 , HCN, and Cl_2 , will be discussed in this section, in addition to the specific structural decisions made, such as material selection and core configuration. The results and analysis of our findings will be presented in Section 3, which will demonstrate the sensor's effectiveness in detecting trace levels of toxic gases. This section will provide comparative evaluations of sensitivity and confinement loss under a variety of conditions, which will be substantiated by in-depth analysis and graphical data. During the discussion, we will emphasize the sensor's potential practical applications and high accuracy, as well as how our results compare to or surpass current benchmarks. Lastly, the conclusion will provide a comprehensive overview of the contributions of our research, emphasizing the sensor's superior sensitivity and specificity in the detection of toxic gases. We will also discuss the implications for future research, including potential deployment in real-world environmental monitoring and industrial safety systems and areas for further enhancement.

2- Research Methodology

In this study, we effectively designed and analyzed the anticipated PCF sensor using COMSOL MULTIPHYSICS 6.2 Simulating Programs. We use the finite element method (FEM) for the design of geometry, and MATLAB is used for displaying the graphs representing the optical characteristics. Figure 1-a illustrates a 2D cross-sectional representation of this recommended photonic crystal fiber. This recommended HC-PCF structure has a centrally located, octagonal-shaped core. We use a structured octagonal-shaped hollow core to increase the relative sensitivity in comparison to cores with hexagonal, pentagonal, square, rectangular, etc., shapes. Moreover, the incorporation of a hexagonal core will enable the placement of extra samples in that specific area, hence enhancing the sensing capabilities. We precisely indicate the radius of this octagonal core as C = 3.135P. The cladding region of the suggested design was constructed employing semi-circular trapezoid air holes with a radius of R, where R is equal to 6.175P. M stands for the strut size, which is the width of material between cladding and core holes or the gap between two adjacent air holes. The separation between these two air holes is 0.19 times the P value. In a rectangular perfectly matched layer, the inner layer L_1 features a height of 6.65P and a width of 7.6P, whereas the outer layer L_2 has a height of 7.6P and a width of 8.55P. Within this particular framework, the variable "P" spans from 130 to 220 micro-meters. In the fiber's outer region, rectangular PML is added to minimize back-reflection. The PML absorbs light that escapes from the core at the outer surface of the cladding. The choice of Zeonex as the background material was based on its low absorption and minimal material losses, measuring approximately 0.2 cm^{-1}. Additionally, it maintains a consistent index of refraction equal to 1.53 within the frequency range, which spans from 0.1 to 2 terahertz. Zeonex is chosen as the substance for the sensor due to its superior refractive index as well as transparency in the terahertz frequency spectrum.

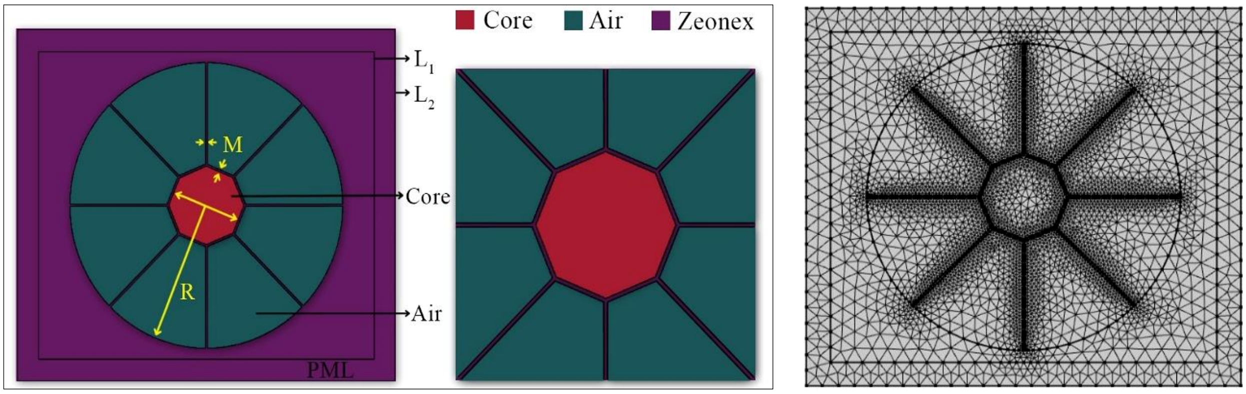

(a) (b)

Figure 1. (a) Geometry of cross-sectional (b) subtle mesh layout of this recommended sensor

The functional details of this presented sensor as well as its associated mesh arrangement are displayed in Figure 1-b. The arrangement of the mesh is critical for accurately representing the intricate light interaction within the fiber. The PCF model requires mesh structuration to effectively control the fiber's optical properties, which include diffraction, light restriction, and mode guidance, which are essential for various optical applications. The mesh analysis consists of 14,198 elements, including 1350 boundary elements and 48 vertex elements. The minimal element quality is 0.566. The design procedure for the hollow-core PCF sensor with an octagonal shape is adequately thorough and supported by evidence. The structure of the sensor is thoroughly described in the article, along with the justification for the octagonal core shape selection, which is meant to optimize light confinement and sensitivity for the detection of harmful gases.

With its semi-circular trapezoid air holes, the cladding zone is purposefully shaped to maximize light interaction with target gas molecules, resulting in reduced effective material loss (EML) and confinement loss (CL). To optimize relative sensitivity for gases like SO_2, HCN, and Cl_2, the paper also describes the material selection and parameter optimization, including core size and operational frequency. Simulations employing the Finite Element Method (FEM) demonstrate the sensor's performance improvements by comparing it to similar ones. The numerical simulations carried out using the finite element approach are explained in detail and with clarity in this article. In order to mimic light propagation within the octagonal hollow-core, it carefully describes the simulation setup, including the material parameters, boundary conditions, and geometric layout of the PCF structure. Important simulation factors that directly affect confinement loss (CL), effective material loss (EML), and RS are described in the article. These parameters include core size, cladding air hole dimensions, and the selected operational frequency in the terahertz region. To guarantee reproducibility and openness, all assumptions made about the distribution of the mode field, material RI, and ambient variables are also made clear. This thorough explanation of the FEM setup and underlying assumptions supports the design's suggested benefits for high-sensitivity dangerous gas detection and strengthens the validity of the simulation findings.

Using an intensity scale, Figure 2-a shows the PCF's internal electromagnetic field distribution under optimal design parameters for the x-polarization mode. This presentation showcases the relationship between the intensity of light and the specific substance being analyzed in the core area, as well as the corresponding figures for SO_2, HCN, and Cl_2 under the given geometrical parameters at a frequency of 1.4 THz. These results show that the applied analytes interact significantly with the concentrated electric field within the core area. On the other hand, the cladding area shows negligible interaction.

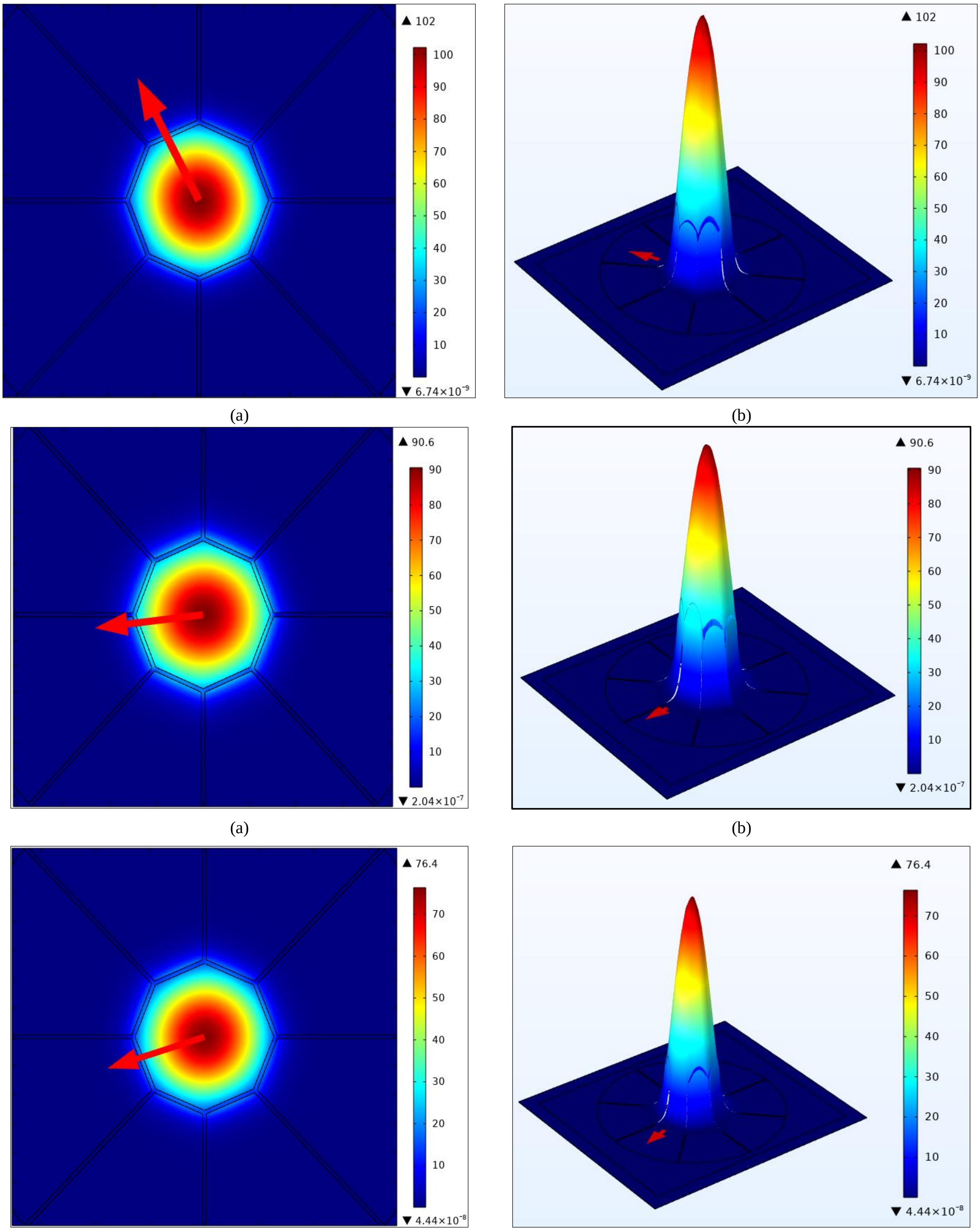

Figure 2. (I): Manifesting the distribution of SO_2 (a) Power (b) Density, (II): Manifesting the distribution of HCN (a) Power (b) Density, (III): Manifesting the distribution of Cl_2 (a) Power (b) Density

The density distribution describes how a material spreads across this sensor. This demonstrates the influence of both innermost and outermost components, as well as the material's functional fibers, on its stiffness. Understanding granular scattering is critical for manufacturing photonic crystal fibers with directional features, certain accountability, or reactions to external influence in applications such as tracking and telecommunication. The quantity of energy delivered or generated per unit volume, area, or mass is referred to as power density. Particularly in situations when weight or space is restricted, it is frequently used to compare the effectiveness of energy sources, batteries, and devices. In applications like mobile electronics and electric cars, where small and effective energy output is crucial, high power density is preferred. The mass of a substance per unit volume is called its density, and it shows how dense its particles are. It is computed as the mass to volume ratio and is commonly given in kilograms per cubic meter (kg/m^3) or grams per cubic centimetre (g/cm^3). Particles with high densities are densely packed, whereas those with low densities are more widely distributed. The flowchart of the research methodology that was used to achieve the study's aims is shown in Figure 3.

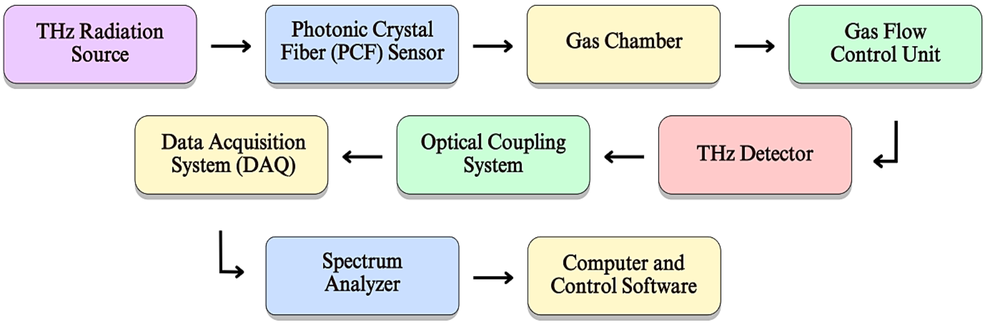

Figure 3. **The flowchart delineated this methodology**

A system for THz radiation detection and analysis is shown in the flow chart. The first step is transmission, where the THz radiation source travels via a gas chamber, photonic crystal fiber (PCF) sensor, and THz detector. Second, Sensing and Acquisition: The signal is sent from the PCF sensor to the THz detector via the optical coupling mechanism. The THz detector's data is collected via the data acquisition (DAQ) system. Third, Control and Analysis: The computer and control software oversee the overall system operation and analysis, while the spectrum analyzer looks at the THz radiation spectrum. The gas chamber may modulate or interact with the THz signal in this system, which enables the production, detection, and spectral analysis of THz radiation. The integrated hardware is used to collect, process, and manage the data.

3- Results and Analyses

For the purpose of detecting poisonous gases (SO_2, HCN, and Cl_2) in the terahertz (THz) band, the theoretical approach in this study is focused on improving PCF structure to obtain high sensitivity and minimal confinement loss. In order to improve the selective detection of gas molecules because of their distinct absorption and scattering properties, we first theoretically simulate the PCF design using the principles of light-gas interaction in the THz band. Zeonex, a low-loss, high-stability material, is used in our method to help achieve high sensitivity and strong light confinement at THz frequencies. This research utilizes FEM to analyze the guiding properties of this recommended framework. We employ FEM to resolve Maxwell's formulas in a rectangular perfectly matched layer (PML) and assess the suggested sensor through innumerable simulations. In order to guarantee the sensor's outstanding performance for real-world dangerous gas detection applications, the theoretical underpinning thus integrates a careful selection of materials, structural optimization, and sophisticated computational approaches. Geometrical and refractive index (RI) values are utilized to evaluate the refraction properties of each component through calculations. This approach improves the reliability of complex PCF setup evaluations, making it simpler and more effective for many optoelectronic applications.

The recommended approach is being replicated using COMSOL software in order to clarify detection characteristics, including spot size, numerical aperture, effective area, confinement loss, relative sensitivity, and effective material loss. In this simulation, we utilized a frequency spectrum spanning from 0.6 to 2.4 Terahertz as well as a pitch range of 130 µm to 220 µm to detect SO_2 (RI = 1.3396), HCN (RI = 1.2675), and Cl_2 (RI = 1.3834). The sensor's performance measures, such as numerical aperture, sensitivity, EML, and CL, are thoroughly and clearly explained in the article. It explains how each parameter relates to the effectiveness of the sensor, especially in improving the terahertz range of gas detection accuracy. The calculation of relative sensitivity and its importance in detecting low concentrations of gases such as SO_2 , HCN, and Cl_2 are explained in depth in the article. It delves deeper into NA, talking about how light confinement in the core is impacted, which has an immediate effect on sensitivity. The paper also discusses EML and CL, describing how they depict light leakage and absorption losses, respectively, and how minimizing them enhances the sensor's high performance. These explanations are accompanied by simulation results that demonstrate the sensor's efficacy in comparison to earlier designs and validate the optimization of each statistic. This method not only closes gaps in the literature but also lays the foundation for increased dependability and specificity in practical applications. Relative sensitivity is defined as the ratio of fractional power transmitted across the core of the sample being sensed to the entire electromagnetic wave power transmitted across the entire photonic crystal fiber (core + cladding). The degree of interaction between light and analyte is strongly linked to the RS of the analyte in a THz photonic crystal fiber. Sensitivity depends on the absorption coefficient at a given frequency. The interaction between light and analyte can be determined using the Beer-Lambert law [38].

$$I(f) = I_0(f) exp[-r\alpha_m l_c] \tag{1}$$

In this context, the symbol I(f) represents light intensity in the presence of the sensing element, while $I_0(f)$ represents light intensity when the sensor component is not present. In addition, the variables r, α_m, l_c, and f represent relative sensitivity, absorption coefficient, channel length, and operating frequency. The sensing element's absorption coefficient can be computed using [38].

$$A = log\left(\frac{I}{I_0}\right) = -r\alpha_m l_c \tag{2}$$

To assess the sensor efficiency of this proposed fibers, it's essential to compute RS. The calculation is determined by [2]:

$$r = \frac{n_r}{n_{eff}} \times p\% \tag{3}$$

In this instance, n_{eff} refers to the sensing material's effective refractive index, whereas n_r denotes the real refractive index component of same material. The RI (n_r) values for SO_2, HCN, and Cl_2 are 1.3396, 1.2675, and 1.3834, respectively. Moreover, the variable p denotes the percentage of power that light carries, a quantity that is measurable [2].

$$p = \frac{\int_{sample} R_e(E_x H_y - E_y H_x)dxdy}{\int_{total} R_e(E_x H_y - E_y H_x)dxdy} \times 100 \tag{4}$$

In this context, H_x & H_y represent magnetic fields, while E_x & E_y represent electric field components of guided modes. RS is interpreted as a variation in a frequency spectrum spanning from 0.6 to 2.4 terahertz, as seen in Figure 4-a. Another side, Figure 4-b, illustrates how a change in pitch from 130 µm to 220 µm might affect the spectrum of integer bands in RS.

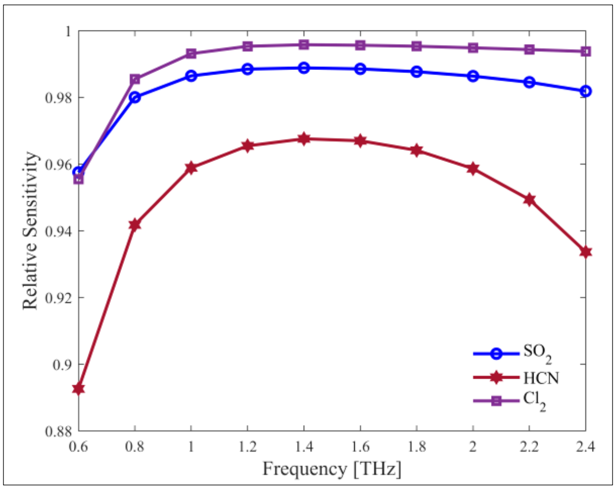

(a)

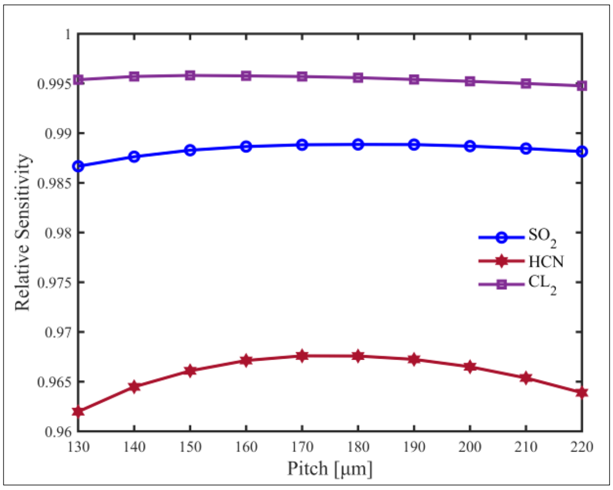

(b)

Figure 4. The recommended fiber's relative sensitivity to different toxic gases: (a) operating frequencies at a fixed pitch during P = 170 µm and (b) various pitches at f = 1.4 THz

Figure 4 shows how the proposed sensor's sensing characteristics have changed. Increased sensitivity values assure the effectiveness of a PCF sensor. Cl_2 maintains the highest relative sensitivity throughout most frequencies, peaking around 1.4-1.6 THz and staying close to 0.99. SO_2 follows a similar pattern to Cl_2 but with slightly lower values, reaching maximum sensitivity around 1.4 THz. HCN shows notably lower sensitivity than the other compounds, with a more pronounced peak at 1.4-1.6 THz before declining sharply after 2.0 THz. Cl_2 exhibits the highest sensitivity of 99.58% operating at a frequency of 1.4 terahertz and with a pitch of 170 micro-meters, while SO_2 and HCN have sensitivities of 98.88% and 96.75%, respectively.

Optical sensors experience losses when used in certain application domains. The primary factors that significantly impact these sensors are effective material loss and confinement loss. Therefore, it is imperative to have a flawless mechanism in place to accurately measure these losses. Confinement loss is defined as the efficiency of a PCF in containing light within the central region of its core. Maintaining a significant property is crucial for designing an efficient PCF. Minimal confinement loss is essential for achieving improved sensing capabilities and minimizing power loss. The Equation 5 is utilized for determining confinement loss [32].

$$L_c = \frac{40\pi}{ln(10)\lambda} img(n_{eff}) \times \frac{10^6 dB}{m} \tag{5}$$

Let f represent the operating frequency, λ denote the real wavelength, and img(n_{eff}) represent the complex effective RI's imaginary part. CL is interpreted as variation in a frequency spectrum spanning from 0.6 to 2.4 terahertz, as illustrated in Figure 5-a. Another side, Figure 5-b, demonstrates how a change in pitch from 130 µm to 220 µm might affect the spectrum of integer bands in CL.

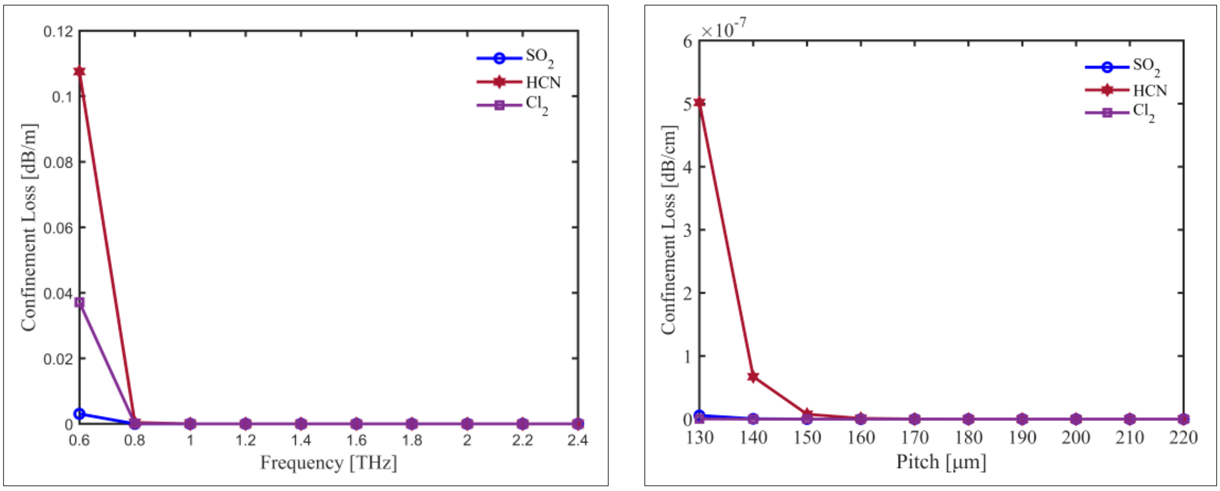

(a) (b)

Figure 5. The recommended fiber's confinement loss to different toxic gases: (a) operating frequencies at a fixed pitch during P = 170 μm and (b) various pitches at f = 1.4 THz

Both figures demonstrate a decreasing trend in confinement loss as frequency and pitch increase. The primary cause of this behaviour is the phenomenon of light propagation with increased confinement in the core zones. Increasing the core's size facilitates the transmission of more light, thereby enhancing the zones where light as well as specific analytes of interest interact. This leads to a more significant reduction in confinement loss, as illustrated in Figure 5. HCN exhibits a comparatively higher CL compared to the other two analytes, SO_2 and Cl_2, which have lower CL values than HCN within their respective operating ranges. At 0.6 THz, HCN exhibits a sharp peak in confinement loss (0.11 dB/m), which quickly drops to almost nil above 0.8 THz. at 0.6 THz, Cl_2 exhibits a significant loss (0.04 dB/m), which rapidly decreases to negligible levels after 0.8 THz. Of the three chemicals, SO_2 has the most stable behaviour, maintaining a constant low confinement loss at all frequencies. For SO_2, HCN, and Cl_2, the corresponding values of CL are 3.56×10^{-12} cm^{-1}, 1.57×10^{-10} cm^{-1}, and 3.09×10^{-12} cm^{-1} operating at a frequency of 1.4 terahertz and with a pitch of 170 micro-meters.

EML stands for the amount of absorbance that background material undergoes. Losses of this nature arise in PCF devices as a result of employing microstructure materials. It is feasible to calculate the effective material loss using the Equation 6 [33]:

$$\alpha_{eff} = \frac{(\frac{\varepsilon_0}{\mu_0})^{\frac{1}{2}} \int_{mat} n_{mat}|E|^2 \alpha_{mat} dA}{2\int_{all} S_z dA} \tag{6}$$

where μ_0 and ϵ_0 indicate relative permeability and permittivity of empty space, respectively. The refractive index is denoted as n_{mat}, the material's absorption coefficient as αmat, the Poynting vector's z-direction component as S_z, and the intensity of the electric field as E. EML is interpreted as a variation in RS, which is interpreted as a frequency spectrum spanning from 0.6 to 2.4 terahertz, as illustrated in Figure 6-a. Another side, Figure 6-b, demonstrates how a change in pitch from 130 μm to 220 μm might affect the spectrum of integer bands in EML.

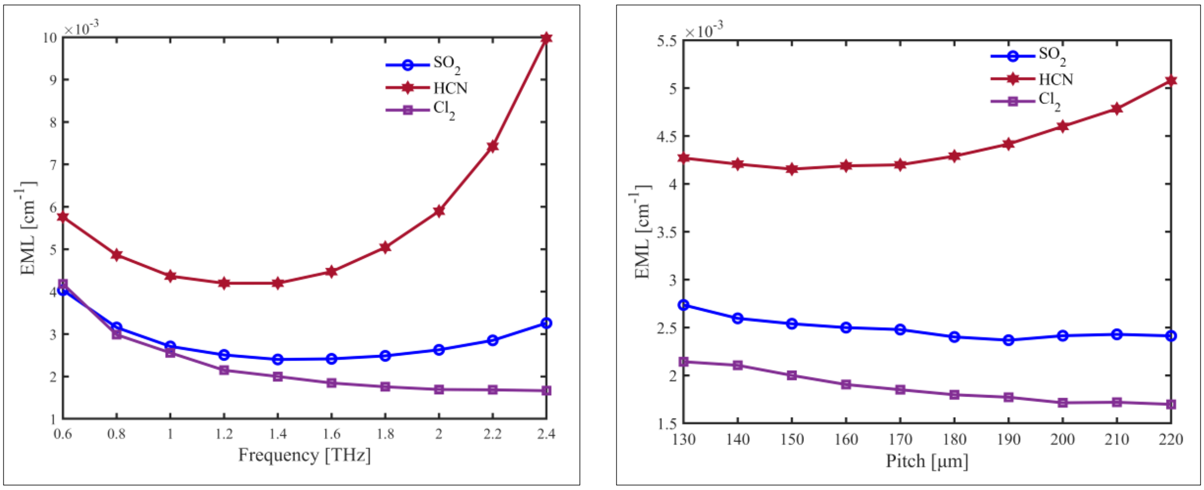

(a) (b)

Figure 6. The recommended fiber's effective material loss to different toxic gases: (a) operating frequencies at a fixed pitch during P = 170 μm (b) various pitches at f = 1.4 Terahertz

In a HC-PCF framework, the electromagnetic wave is stronger and stays firmly confined within the core region, which makes it less likely that light and matter will interact. This leads to a reduction in EML. This article demonstrates that Cl_2's PCF geometry has an incredibly few EML equal to 0.0020 cm^{-1} operating at a frequency of 1.4 terahertz and with a pitch of 170 micrometers. On the other hand, SO_2 and HCN's PCF geometries have losses of 0.2402 cm^{-1} and 0.4199 cm^{-1}, respectively, which are greater than Cl_2. HCN exhibits a U-shaped curve with a minimum of about 1.4 THz and the highest EML values. With lower quantities, SO_2 exhibits a similar U-shaped pattern, with a minimum observed around 1.4-1.6 THz. Overall, Cl_2 has the lowest values, progressively declining before leveling out above 2 THz.

The term "total loss" refers to the complete failure of a PCF sensor to function or produce accurate readings. A variety of factors, such as electricity outages, physical damage, and sensor malfunctions, can cause this. If a PCF sensor has undergone total loss, it is incapable of detecting or registering any alterations in pressure; essentially, it is rendered completely non-functional for any intended use. The Equation 7 is used to calculate total loss [39].

$$TL \equiv EML + CL \tag{7}$$

In this context, EML stands for Effective Material Loss, and CL refers to Confinement Loss. TL is interpreted as a variation in a frequency spectrum spanning from 0.6 to 2.4 terahertz, as illustrated in Figure 7-a. Another side, Figure 7-b demonstrates how a change in pitch from 130 µm to 220 µm might affect the spectrum of integer bands in TL.

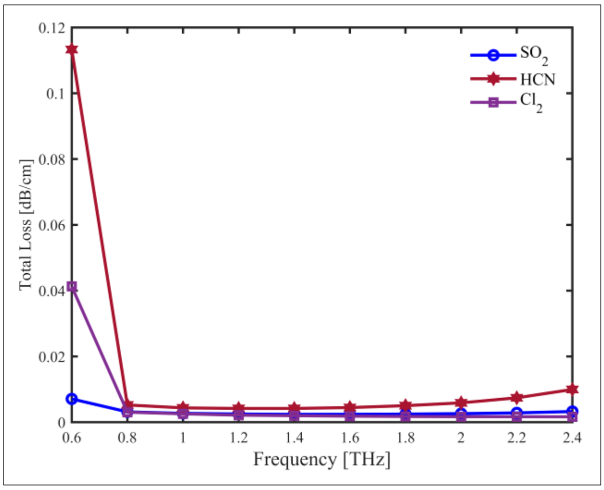

(a)

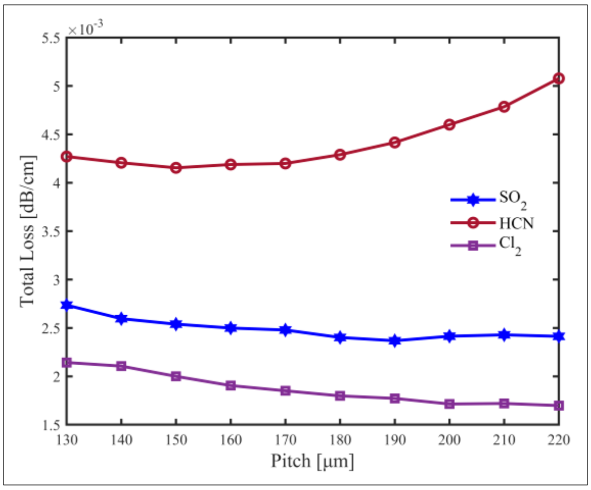

(b)

Figure 7. The recommended fiber's total loss to different toxic gases: (a) operating frequencies at a fixed pitch during P = 170 µm and (b) various pitches at f = 1.4 THz

While SO_2 and Cl_2 both have lower total loss values than HCN within their respective operating ranges, HCN shows a relatively higher total loss. At 0.6 THz (about 0.11 dB/cm), HCN exhibits the largest total loss; however, above 0.8 THz, it lowers down rapidly to stabilize with other compounds. Cl_2 rapidly drops to maintain the lowest loss above 1.0 THz after beginning at roughly 0.04 dB/cm at 0.6 THz. In contrast to the other chemicals, SO_2 exhibits quite little fluctuation in its low loss values across the frequency range. Operating at a frequency of 1.4 terahertz and with a pitch of 170 micro-meters, the corresponding TL values for SO_2, HCN, and Cl_2 are 2.40×10^{-3} cm^{-1}, 4.19×10^{-3} cm^{-1}, and 2.005×10^{-3} cm^{-1}.

The spot size (SS) refers to the effective area within a photonic crystal fiber that restricts and propagates light through the fiber. The core and cladding's differences in RI, band gap layout in photonics, influence the spot size in PCF. A larger spot size implies increased light scattering, whereas a smaller spot size indicates more stringent confinement and higher spatial resolution. The following formula applies mathematics to determine a spot size [40].

$$W_{eff} = R \times (.65 \times 1.619 \times V^{-1.5} + 2.789 \times V^{-6}) \tag{8}$$

Here, R represents the core's radius, whereas V represents frequency level that has been changed. SS is interpreted as a variation in a frequency spectrum spanning from 0.6 to 2.4 terahertz, as illustrated in Figure 8-a. Another side, Figure 8-b demonstrates how a change in pitch from 130 µm to 220 µm might affect the spectrum of integer bands in SS.

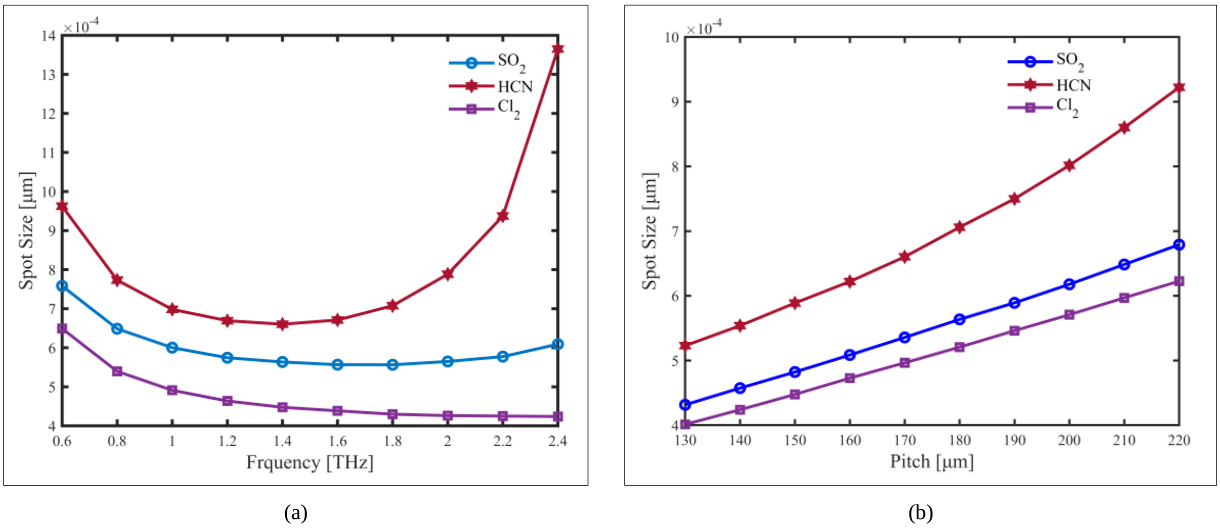

Figure 8. **The recommended fiber's spot size to different toxic gases: (a) operating frequencies at a fixed pitch during P = 170 µm (b) various pitches at f = 1.4 Terahertz**

The characteristic can be derived from the spot size measurements depicted in Figure 7. An efficient PCF sensor often favours a smaller spot size. The graph displays the correlation between spot size (4.14×10^{-4} µm) and frequency (0.6-2.4 THz) for three molecules: Cl_2, HCN, and SO_2. The spot size of Cl_2 steadily decreases as the frequency increases, whereas SO_2 and HCN exhibit U-shaped curves with minimum values at about 1.6 THz. At 2.4 THz, HCN shows the most significant shift, with the greatest spot size of almost 13.5×10^{-4}µm. Operating at a frequency of 1.4 terahertz and with a pitch of 170 micrometers, the SS of Cl_2 is the lowest at 4.47×10^{-4} cm^{-1}. In the same frequency range, SO_2 and HCN have SS values of 5.63×10^{-4} cm^{-1} and 6.60×10^{-4} cm^{-1}.

Numerical aperture quantitatively measures a photonic crystal fiber's capability to collect light. The difference in RI between cladding and core quantifies NA. In situations where there is a need for extensive sensing, a larger numerical aperture (NA) is anticipated. The calculation for this NA can be determined as follows [2].

$$NA = \frac{1}{\sqrt{1+\frac{\pi A_{eff} f^2}{c^2}}} \approx \frac{1}{\sqrt{1+\frac{\pi A_{eff}}{\lambda^2}}} \tag{9}$$

The symbol A_{eff} denotes the effective area, and light speed as well as the operating frequency are represented by the symbols c and f, respectively. NA is interpreted as variation in a frequency spectrum spanning from 0.6 to 2.4 terahertz, as illustrated in Figure 9-a. Another side, Figure 9-b demonstrates how a change in pitch from 130 µm to 220 µm might affect the spectrum of integer bands in NA.

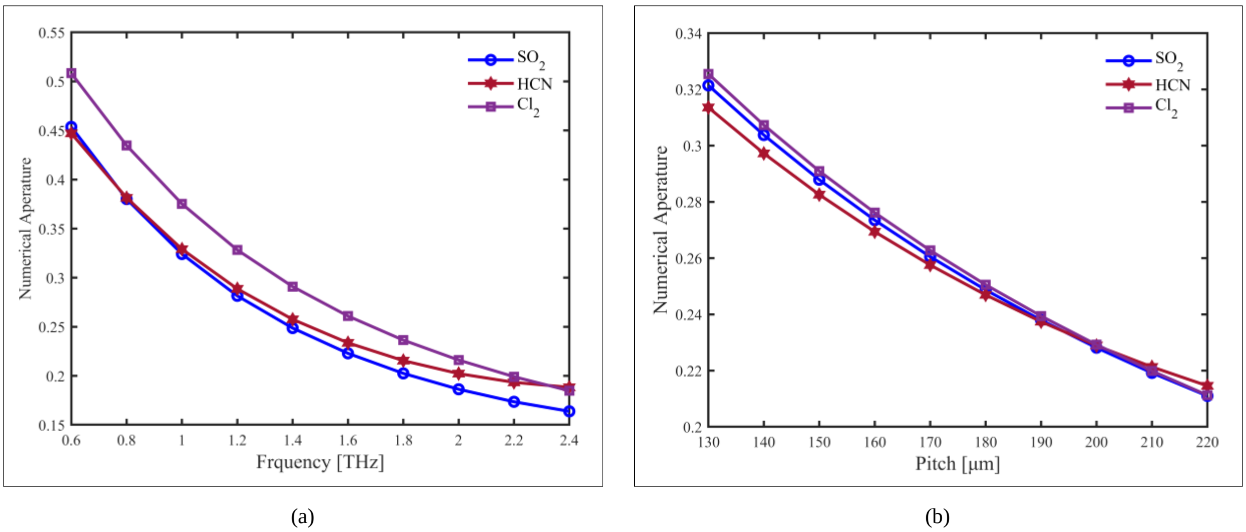

Figure 9. **The recommended fiber's numerical aperture to different toxic gases: (a) operating frequencies at a fixed pitch during P = 170 µm (b) various pitches at f = 1.4 Terahertz**

Analyzing the numerical aperture is crucial because it governs the incident light's properties, and a higher numerical aperture guarantees improved sensor performance. Across the majority of the frequency range, Cl_2 exhibits the largest numerical aperture values. The curves for SO_2 and HCN are almost the same until they start to somewhat diverge at around 1.6 THz. As frequency rises, all three chemicals exhibit a steady declining trend, with their lowest values occurring at 2.4 THz. Operating at a frequency of 1.4 terahertz and with a pitch of 170 micrometers, Cl_2 exhibits the highest NA value of 0.2909, whereas SO_2 and HCN have NA values of 0.2487 and 0.2575, respectively.

The photonic device's effective area (EA) at the THz frequency is a critical parameter for mitigating the nonlinear effect and balancing dispersion. The effective area refers to the specific region within the fiber where the interaction between light and matter occurs. This area denotes the operational range of a sensor by quantifying the density of light. Using Equation 9, the value of A_{eff} is determined [41]:

$$A_{eff} = \frac{[\int I(r)rdr]^2}{[\int I^2(r)rdr]^2} \tag{10}$$

The variable $I(r)$ denotes the magnitude of the optical field at a radial distance r from the fiber's center. EA is interpreted as a variation in a frequency spectrum spanning from 0.6 to 2.4 terahertz, as illustrated in Figure 10-a. Another side, Figure 10-b demonstrates how a change in pitch from 130 μm to 220 μm might affect the spectrum of integer bands in EA.

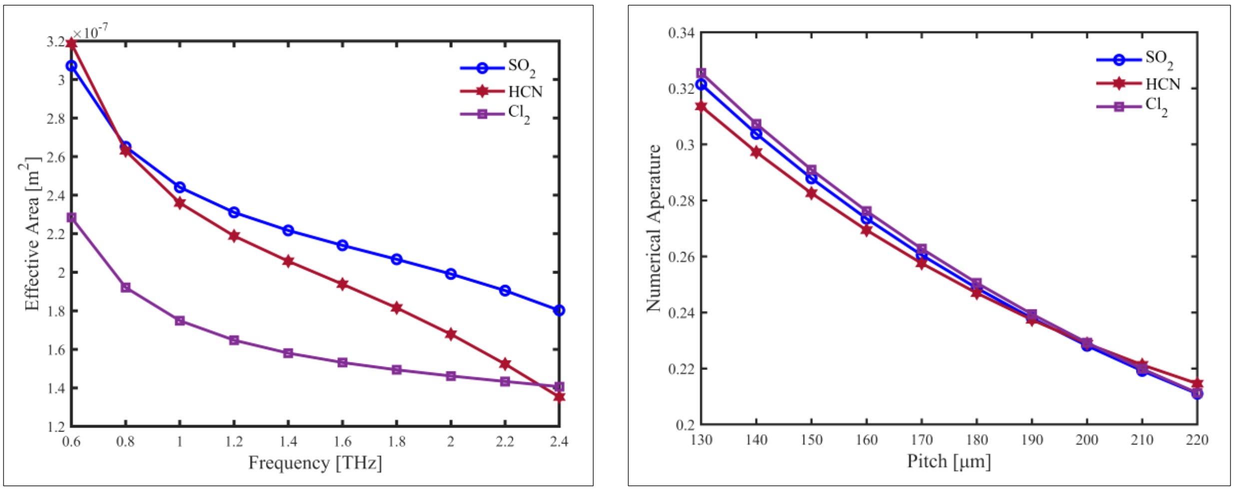

(a) (b)

Figure 10. The recommended fiber's effective area to different toxic gases: (a) operating frequencies at a fixed pitch during P = 170 μm (b) various pitches at f = 1.4 Terahertz

The precise location where light is limited is determined by measuring the effective area. In our study, we report the A_{eff} features obtained from the observations in Figure 9. A highly effective PCF sensor typically prefers a smaller value of A_{eff}. Over the majority of frequencies, SO_2 maintains the largest effective area, progressively decreasing from 3.1×10^{-7} to 1.8×10^{-7} m^2. After peaking at 3.2×10^{-7} m^2, HCN falls more quickly than SO_2, particularly after 1.4 THz, and converges with Cl_2 at 2.4 THz. Cl_2 exhibits a more gradual drop and continuously lower effective area values, stabilizing at higher frequencies at about 1.4×10^{-7} m^2. Operating at a frequency of 1.4 terahertz and with a pitch of 170 micrometres, A_{eff} of Cl_2 is the lowest at 1.58×10^{-7} m^2. In the same frequency range, SO_2 and HCN have A_{eff} values of 2.21×10^{-7} m^2 and 2.05×10^{-7} m^2, respectively.

A comparison between our suggested model and existing research provides Table 1. Every analysis is conducted specifically for PCF sensing that operates within the terahertz frequency range.

The comparative analysis in Table 1 reveals significant advancements in the sensitivity and performance of the newly developed octagonal-core PCF sensor for detecting toxic gases like SO_2, HCN, and Cl_2. Notably, the sensor achieves a peak relative sensitivity of 99.58% for Cl_2 at an operational frequency of 1.4 THz, outperforming previous designs by a considerable margin. For example, Hossain et al. [8] designed a sensor with a maximum sensitivity of 88.5% for KCN at 1.8 THz, while Ferdous et al. [2] and Islam et al. [3] reported respective maximum sensitivities of 87.34% and 89.4% for SO_2 and NaCN, yet with higher confinement losses (CL) and effective material losses (EML). The novel sensor's low confinement loss, at 3.09×10^{-12} dB/m for Cl_2, and minimal EML of 0.0020 cm^{-1} reflect enhanced light confinement and reduced energy dissipation compared to previous models, such as those by Bulbul et al. [12] and Jibon et al. [42], who reported EML values of 0.0066 cm^{-1} and 0.0059 cm^{-1} respectively. Additionally, while designs like that of Shahriyar et al. [43] achieved a high sensitivity of 94.06% for C_6H_6, the created sensor exhibits superior performance across all parameters, particularly in minimizing CL and EML, making it a leading candidate for accurate, high-sensitivity detection of hazardous gases in real-world applications.

Table 1. The study aims to compare the features of recommended and previously released sensors based on PCF

Ref. of list	Shape of PCF	Analyte	Opt. Freq. (THz)	R. Sensitivity (%)	CL (dB/m)	EML (cm^{-1})
PCF [8]	Circular-base air holes having a rectangular-core structure	NaCN	1.8	85.20	1.20×10^{-11}	0.005
		KCN		88.50	1.48×10^{-11}	0.0052
PCF [12]	Elliptical core with hexagonally arranged elliptical and circular air holes	NaCN	1.0	88.64	3.81×10^{-12}	0.0066
		KCN		84.52	9.16×10^{-10}	0.0047
PCF [2]	Heptagonal cladding with circular air holes surrounding the octagonal-shaped HC	SO_2	1.6	87.34	6.81×10^{-4}	0.0593
PCF [3]	Suspension-type cladding has circular-shaped air holes	HCN	1.8	85.8	N/A	0.023
		NaCN		89.4		0.023
		KCN		88.8		0.023
PCF [42]	Rectangular air holes with a core structure in the shape of a rectangle.	HCN	1.8	88.2	1.85×10^{-13}	0.0037
		NaCN		93.0	1.10×10^{-12}	0.0059
		KCN		91.0	3.76×10^{-12}	0.0044
PCF [43]	Octagonal core area is by air holes in the shape of rectangles and circles.	C_6H_6	1.2	94.06	9.95×10^{-22}	0.0148
		SO_3		91.43	1.01×10^{-17}	0.0265
Created PCF Sensor	Octagonal-shaped core, the cladding region has semi-circular trapezoid air holes	SO_2	1.4	98.88	3.56×10^{-12}	0.0024
		HCN		96.75	1.57×10^{-10}	0.0042
		Cl_2		99.58	3.09×10^{-12}	0.0020

The practical implications of each proposed sensor can be understood by evaluating its requirements for fabrication. Extrusion, 3D printing, and sol-gel, stacking, as well as drawing are widely recognized techniques for fabrication. While capillary stacking and sol-gel technologies are viable methods for creating circular micro-structured air cavities, they are not commonly used for producing our suggested sensor. The extrusion process provides flexibility in creating asymmetrical structures of various shapes, such as circular, rectangular, or square. The Max Planck Institute utilizes extrusion and 3D-printing techniques to manufacture a range of intricately structured photonic crystal fibers (PCFs) [44, 45]. Our proposed sensor may be readily fabricated using extrusion or 3D-printing techniques.

4- Conclusion

To detect SO_2, HCN, and Cl_2 gas, a toxic gas sensor with an octagonal core has been constructed using COMSOL Multiphysics. After giving great thought to this issue, we have created our expected detection system with a high probability of accurate identification. Our suggested technique surpasses conventional detection techniques, as shown in Table 1, with regard to sensing effectiveness as well as reliability in sulphur dioxide and other toxic compounds. Following a successful experiment, we discovered that the chlorine sensor we developed has a maximum relative sensitivity of approximately 99.58%. Additionally, we observed negligible values for EML (0.002) and confinement loss (3.094×10^{-12} dB/m) of 1.4 terahertz in frequency. By precisely detecting even the smallest changes in refractive index (RI), the suggested detector will make it possible to detect SO_2, HCN, and Cl_2 - even in trace levels. The quick response of the sensor makes it possible to monitor SO_2, HCN, and Cl_2 levels instantly, which is essential for responding quickly to dangerous situations. In conclusion, the newly introduced PCF detectors are incredibly versatile instruments that offer superior precision and efficacy in accurately detecting SO_2, HCN, and Cl_2 in a variety of situations. This significantly improves the monitoring process. Future research will investigate new materials, redesign the sensor's architecture, and use advanced signal processing techniques to improve the accuracy, dependability, and usefulness of a PCF detector for the detection of harmful gases. Because of its adherence to fabrication procedures and its capacity to detect SO_2, HCN, and Cl_2, we heartily endorse our suggested sensor.

5- Declarations

5-1- Author Contributions

Conceptualization, A.H.M.I.F.; methodology, M.S.H. and A.H.M.I.F.; software, M.S.H., A.H.J., and D.K.; validation, A.H.M.I.F., A.A.M., and M.J.H.; formal analysis, A.H.J. and D.K.; investigation, D.K. and A.A.M.; resources, A.H.M.I.F. and M.J.H.; data curation, M.S.H., A.H.J., and D.K.; writing—original draft preparation, M.S.H., A.H.J., and D.K.; writing—review and editing, A.A.M. and A.H.M.I.F.; visualization, A.A.M. and M.J.H.; supervision, A.H.M.I.F.; project administration, A.H.M.I.F.; funding acquisition, M.J.H. All authors have read and agreed to the published version of the manuscript.

5-2- Data Availability Statement

The data presented in this study are available on request from the corresponding author.

5-3- Funding

The authors received no financial support for the research, authorship, and/or publication of this article.

5-4- Institutional Review Board Statement

Not applicable.

5-5- Informed Consent Statement

Not applicable.

5-6- Conflicts of Interest

The authors declare that there is no conflict of interest regarding the publication of this manuscript. In addition, the ethical issues, including plagiarism, informed consent, misconduct, data fabrication and/or falsification, double publication and/or submission, and redundancies have been completely observed by the authors.

6- References

[1] Khaniabadi, Y. O., Polosa, R., Chuturkova, R. Z., Daryanoosh, M., Goudarzi, G., Borgini, A., Tittarelli, A., Basiri, H., Armin, H., Nourmoradi, H., Babaei, A. A., & Naserian, P. (2017). Human health risk assessment due to ambient PM10 and SO2 by an air quality modeling technique. Process Safety and Environmental Protection, 111, 346–354. doi:10.1016/j.psep.2017.07.018.

[2] Ferdous, A. H. M. I., Mynuddin, M., & Noor, K. S. (2024). High-performance sulphur dioxide sensor: Unveiling the potential of photonic crystal fibre technology. IET Nanodielectrics, 12084. doi:10.1049/nde2.12084.

[3] Islam, M. S., Sultana, J., Dinovitser, A., Ahmed, K., Ng, B. W. H., & Abbott, D. (2018). Sensing of toxic chemicals using polarized photonic crystal fiber in the terahertz regime. Optics Communications, 426, 341–347. doi:10.1016/j.optcom.2018.05.030.

[4] Gessner, M. A., Doran, S. F., Yu, Z., Dunaway, C. W., Matalon, S., & Steele, C. (2013). Chlorine gas exposure increases susceptibility to invasive lung fungal infection. American Journal of Physiology - Lung Cellular and Molecular Physiology, 304(11), 765– 773. doi:10.1152/ajplung.00030.2013.

[5] Huang, T., Hou, Z., Xu, Q., Huang, L., Li, C., & Zhou, Y. (2017). Polymer vesicle sensor for visual and sensitive detection of SO2 in water. Langmuir, 33(1), 340–346. doi:10.1021/acs.langmuir.6b03869.

[6] Zhang, J., Pang, J., Chen, H., Wei, G., Wei, S., Wang, K., & Yan, J. (2023). Theoretical study of 2D PbSe/Bi2Se3 heterojunctions as gas sensors for the detection of SO2 and Cl2. Physica Scripta, 98(9), 95905. doi:10.1088/1402-4896/aceabf.

[7] Erdemir, S., & Malkondu, S. (2020). On-site and low-cost detection of cyanide by simple colorimetric and fluorogenic sensors: Smartphone and test strip applications. Talanta, 207, 120278. doi:10.1016/j.talanta.2019.120278.

[8] Hossain, M. B., Podder, E., Bulbul, A. A. M., Mondal, H. S., Raihan, M., & Islam, M. T. (2019). Identification of Cyanide within Hollow Core Photonics Crystal Fiber. 2019 10th International Conference on Computing, Communication and Networking Technologies, ICCCNT 2019, 1–4. doi:10.1109/ICCCNT45670.2019.8944499.

[9] Timofeyenko, Y. G., Rosentreter, J. J., & Mayo, S. (2007). Piezoelectric quartz crystal microbalance sensor for trace aqueous cyanide ion determination. Analytical Chemistry, 79(1), 251–255. doi:10.1021/ac060890m.

[10] Yu, Y., Shu, T., & Dong, C. (2017). A convenient colorimetric and ratiometric fluorescent probe for detection of cyanide based on BODIPY derivative in aqueous media. Analytical Chemistry Research, 12, 34–39. doi:10.1016/j.ancr.2017.01.004.

[11] Jibon, R. H., Bulbul, A. A. M., & Rahaman, M. E. (2021). Numerical Investigation of the Optical Properties for Multiple PCF Structures in the THz Regime. Sensing and Bio-Sensing Research, 32, 100405. doi:10.1016/j.sbsr.2021.100405.

[12] Bulbul, A. A. M., Jibon, R. H., Awal, M. A., Podder, E., Mondal, H. S., Ahmed, M. S., Hossain, M. B., Hasan, M. M., & Saha, A. (2020). Toxic Chemicals Detection using Photonic Crystal Fiber in THz Regime. 2020 11th International Conference on Computing, Communication and Networking Technologies, ICCCNT 2020, 1–5. doi:10.1109/ICCCNT49239.2020.9225544.

[13] Monro, T. M., Belardi, W., Furusawa, K., Baggett, J. C., Broderick, N. G. R., & Richardson, D. J. (2001). Sensing with microstructured optical fibres. Measurement Science and Technology, 12(7), 854–858. doi:10.1088/0957-0233/12/7/318.

[14] Islam, M. S., Sultana, J., Rifat, A. A., Dinovitser, A., Wai-Him Ng, B., & Abbott, D. (2018). Terahertz sensing in a hollow core photonic crystal fiber. IEEE Sensors Journal, 18(10), 4073–4080. doi:10.1109/JSEN.2018.2819165.

[15] Shephard, J. D., MacPherson, W. N., Maier, R. R. J., Jones, J. D. C., Hand, D. P., Mohebbi, M., George, A. K., Roberts, P. J., & Knight, J. C. (2005). Single-mode mid-IR guidance in a hollow-core photonic crystal fiber. Optics Express, 13(18), 7139. doi:10.1364/opex.13.007139.

[16] Atiqullah, S. M., Palit, A., Reja, M. I., Akhtar, J., Fatema, S., & Absar, R. (2019). Detection of harmful food additives using highly sensitive photonic crystal fiber. Sensing and Bio-Sensing Research, 23, 100275. doi:10.1016/j.sbsr.2019.100275.

[17] Niger, M., Reja, M. I., Akhtar, J., Jahan, N., Absar, R., & Fatema, S. (2019). Modified dodecagonal PCF sensor with high sensitivity for detecting harmful chemical compounds used in poultry feed. 2019 5th International Conference on Advances in Electrical Engineering, ICAEE 2019, 530–535. doi:10.1109/ICAEE48663.2019.8975607.

[18] Liu, H.-B., Chen, Y., Bastiaans, G. J., & Zhang, X.-C. (2006). Detection and identification of explosive RDX by THz diffuse reflection spectroscopy. Optics Express, 14(1), 415. doi:10.1364/opex.14.000415.

[19] Gavdush, A. A., Chernomyrdin, N. V., Malakhov, K. M., Beshplav, S.-I. T., Dolganova, I. N., Kosyrkova, A. V., Nikitin, P. V., Musina, G. R., Katyba, G. M., Reshetov, I. V., Cherkasova, O. P., Komandin, G. A., Karasik, V. E., Potapov, A. A., Tuchin, V. V., & Zaytsev, K. I. (2019). Terahertz spectroscopy of gelatin-embedded human brain gliomas of different grades: a road toward intraoperative THz diagnosis. Journal of Biomedical Optics, 24(2), 1. doi:10.1117/1.jbo.24.2.027001.

[20] Mittleman, D. M. (2018). Twenty years of terahertz imaging. Optics Express, 26(8), 9417. doi:10.1364/oe.26.009417.

[21] Luk, K. M., Zhou, S. F., Li, Y. J., Wu, F., Ng, K. B., Chan, C. H., & Pang, S. W. (2017). A microfabricated low-profile wideband antenna array for terahertz communications. Scientific Reports, 7(1), 1268. doi:10.1038/s41598-017-01276-4.

[22] Fischer, B., Hoffmann, M., Helm, H., Modjesch, G., & Jepsen, P. U. (2005). Chemical recognition in terahertz time-domain spectroscopy and imaging. Semiconductor Science and Technology, 20(7), 246. doi:10.1088/0268-1242/20/7/015.

[23] Arif, M. F. H., Ahmed, K., Asaduzzaman, S., & Azad, M. A. K. (2016). Design and optimization of photonic crystal fiber for liquid sensing applications. Photonic Sensors, 6(3), 279–288. doi:10.1007/s13320-016-0323-y.

[24] Mohamed Nizar, S., Caroline, E., & Krishnan, P. (2021). Design and Investigation of a High-Sensitivity PCF Sensor for the Detection of Sulfur Dioxide. Plasmonics, 16(6), 2155–2165. doi:10.1007/s11468-021-01473-y.

[25] Podder, E., Hossain, M. B., Jibon, R. H., Bulbul, A. A. M., & Mondal, H. S. (2019). Chemical sensing through photonic crystal fiber: sulfuric acid detection. Frontiers of Optoelectronics, 12(4), 372–381. doi:10.1007/s12200-019-0903-8.

[26] Sultana, J., Islam, M. S., Ahmed, K., Dinovitser, A., Ng, B. W.-H., & Abbott, D. (2018). Terahertz detection of alcohol using a photonic crystal fiber sensor. Applied Optics, 57(10), 2426. doi:10.1364/ao.57.002426.

[27] Abbaszadeh, A., Makouei, S., & Meshgini, S. (2022). New hybrid photonic crystal fiber gas sensor with high sensitivity for ammonia gas detection. Canadian Journal of Physics, 100(2), 129–137. doi:10.1139/cjp-2021-0016.

[28] Nizar, S. M., Caroline, B. E., & Krishnan, P. (2022). Photonic crystal fiber sensor for the detection of hazardous gases. Microsystem Technologies, 28(9), 2023–2035. doi:10.1007/s00542-022-05341-5.

[29] Ahmed, K., Ahmed, F., Roy, S., Paul, B. K., Aktar, M. N., Vigneswaran, D., & Islam, M. S. (2019). Refractive Index-Based Blood Components Sensing in Terahertz Spectrum. IEEE Sensors Journal, 19(9), 3368–3375. doi:10.1109/JSEN.2019.2895166.

[30] Islam, M. S., Sultana, J., Ahmed, K., Islam, M. R., Dinovitser, A., Ng, B. W. H., & Abbott, D. (2018). A novel approach for spectroscopic chemical identification using photonic crystal fiber in the terahertz regime. IEEE Sensors Journal, 18(2), 575–582. doi:10.1109/JSEN.2017.2775642.

[31] Islam, M. S., Sultana, J., Dinovitser, A., Ahmed, K., Islam, M. R., Faisal, M., Ng, B. W. H., & Abbott, D. (2017). A novel Zeonex based photonic sensor for alcohol detection in beverages. 2nd IEEE International Conference on Telecommunications and Photonics, ICTP 2017, 2017-December, 114–118. doi:10.1109/ICTP.2017.8285905.

[32] Mahmud, S. S., Islam, M. T., & Atiqullah, S. M. (2019). Poisonous Chemical Sensing Using Highly Sensitive Terahertz Photonic Crystal Fiber Sensor. 2019 4th International Conference on Electrical Information and Communication Technology, EICT 2019, 1–5. doi:10.1109/EICT48899.2019.9068856.

[33] Hossain, M. B., Podder, E., Bulbul, A. A. M., & Mondal, H. S. (2020). Bane chemicals detection through photonic crystal fiber in THz regime. Optical Fiber Technology, 54, 102102. doi:10.1016/j.yofte.2019.102102.

[34] Hossain, M. S., Mollah, M. S. H., Rahman, M. H., & Sen, S. (2024). Design and performance analysis of PCF-based octagonal chemical sensor to detect benzene, ethanol, and water in terahertz spectrum. Results in Optics, 14, 100599. doi:10.1016/j.rio.2023.100599.

[35] Mahbub, S. M., Shamim, M. H. M., & Sagor, R. H. (2024). Gas Detection Utilizing Soliton Effect Pulse Compression in a Hollow Core Photonic Crystal Fiber. Proceedings - 6th International Conference on Electrical Engineering and Information & Communication Technology, ICEEICT 2024, 308–312. doi:10.1109/ICEEICT62016.2024.10534440.

[36] Pourfathi Fard, A., Makouei, S., Danishvar, M., & Danishvar, S. (2024). The Design of a Photonic Crystal Fiber for Hydrogen Cyanide Gas Detection. Photonics, 11(2), 178. doi:10.3390/photonics11020178.

[37] Islam, M. S., Ferdous, A. H. M. I., Noor, K. S., & Bani, M. M. (2024). Designing hollow-core PCF sensors for high-performance terahertz detection of NaCN and KCN. Heliyon, 10(18), e37681. doi:10.1016/j.heliyon.2024.e37681.

[38] Rahman, M. M., Mou, F. A., Bhuiyan, M. I. H., & Islam, M. R. (2020). Photonic crystal fiber based terahertz sensor for cholesterol detection in human blood and liquid foodstuffs. Sensing and Bio-Sensing Research, 29, 100356. doi:10.1016/j.sbsr.2020.100356.

[39] Ferdous, A. I., Rani, L., Islam, M. S., Noor, K. S., Roy, S., Eid, M. M., & Rashed, A. N. Z. (2024). Development and enhancement of PCF-based sensors for terahertz-frequency region breast cancer cell detection. Cell Biochemistry and Biophysics, 82(3), 2837-2852. doi:10.1007/s12013-024-01399-2.

[40] Iftekharul Ferdous, A. H. M., Islam, M. S., Noor, K. S., Bani, M. M., Badhon, N. U., & Enzamam-Ul-Haque, M. (2024). Harnessing THz technology: biosensor for highly accurate cervical cancer cell detection via refractive index. Cell Biochemistry and Biophysics, 82(3), 2095-2106. doi:10.1007/s12013-024-01318-5.

[41] Shobug, M. A., Noor, K. S., Sagaya Raj, A. G., Ramkumar, G., Padmanaban, P., Mallan, S., ... & Rashed, A. N. Z. (2024). Fuel quality assurance based on hybrid hexagonal circular hollow core PCF sensing through management of terahertz region operation. Journal of Optics, 1-16. doi:10.1007/s12596-024-01756-7.

[42] Jibon, R. H., Ahmed, M., Shaikh, M. M., Tooshil, A., Alahe, M. A., & Hassan, M. M. (2021). Cyanide Detection with PCF in the THz Region: Composition and Performance Perusal. 2021 International Conference on Science & Contemporary Technologies, ICSCT 2021, 1–5. doi:10.1109/ICSCT53883.2021.9642694.

[43] Shahriyar, F., Nasif, M. A., Gafur, A., Faisal, M. M. A., Samudra, D. B., & Rashid, S. Z. (2024). Quantitative Analysis of Photonic Crystal Fiber Gas Sensors: Sensitivity Metrics for Benzene and Sulfur Trioxide. 2024 3rd International Conference on Advancement in Electrical and Electronic Engineering, ICAEEE 2024, 1–6. doi:10.1109/ICAEEE62219.2024.10561706.

[44] Ebendorff-Heidepriem, H., Schuppich, J., Dowler, A., Lima-Marques, L., & Monro, T. M. (2014). 3D-printed extrusion dies: a versatile approach to optical material processing. Optical Materials Express, 4(8), 1494. doi:10.1364/ome.4.001494.

[45] Yang, T., Ding, C., Ziolkowski, R. W., & Guo, Y. J. (2019). A terahertz (THz) single-polarization-single-mode (SPSM) photonic crystal fiber (PCF). Materials, 12(15), 2442. doi:10.3390/ma12152442.